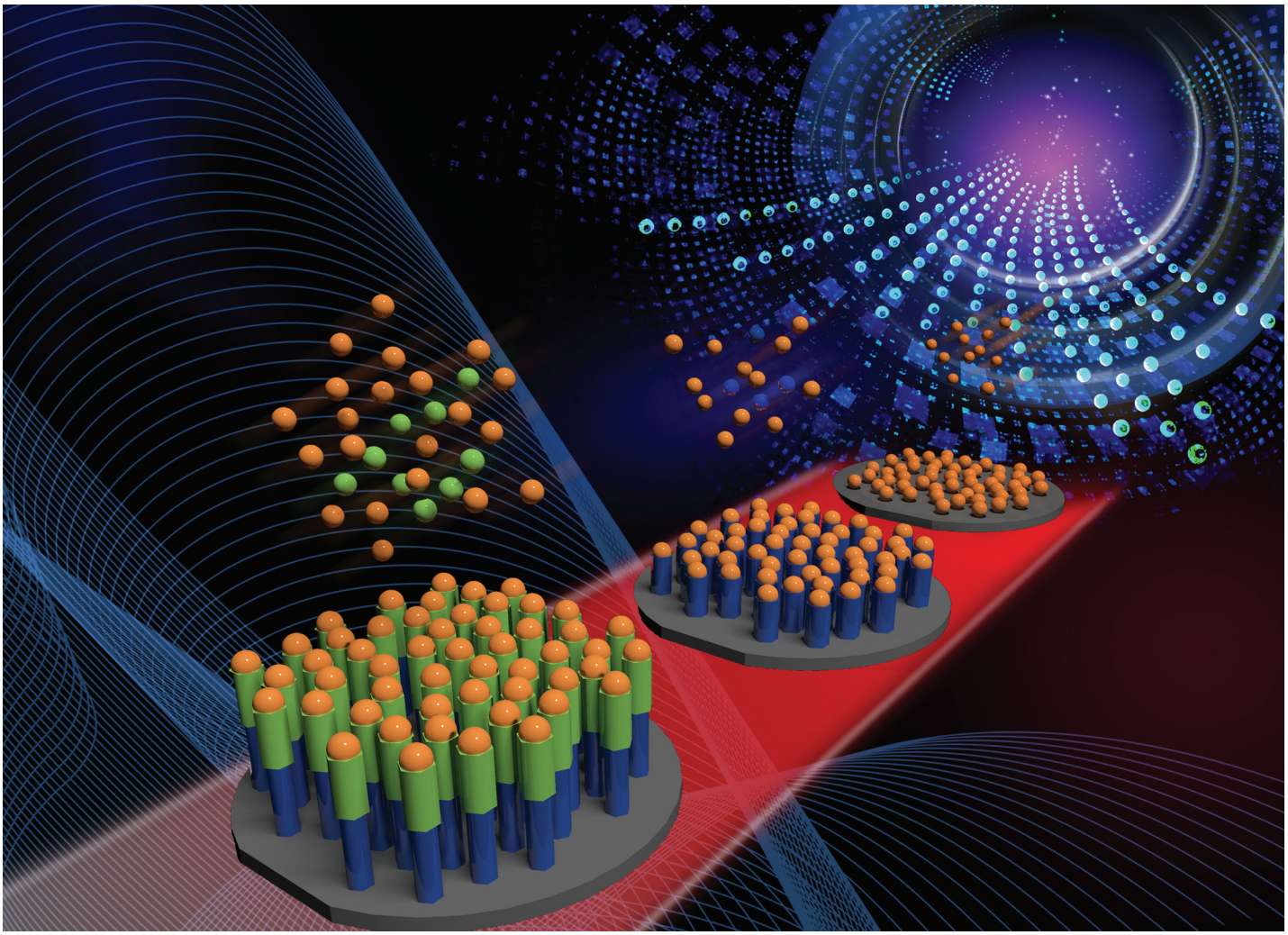

Showcasing research from the Institute of Semiconductors, Chinese Academy of Sciences, Beijing, China.

Two-step fabrication of self-catalyzed Ga-based semiconductor nanowires on Si by molecular-beam epitaxy

For the epitaxial growth of Ga-based III–V semiconductor nanowires (NWs) on Si, Ga droplets could provide a clean and compatible solution in contrast to the common Au catalyst. By a two-step procedure, the successful fabrication of self-catalyzed GaAs and GaSb NWs and also composition-tunable GaAsSb NWs on Si was demonstrated.

As featured in:

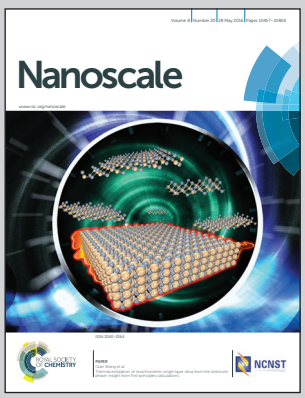

See Jianhua Zhao *et al*. *Nanoscale*, 2016, **8**, 10615.

ROYAL SOCIETY OF CHEMISTRY

www.rsc.org/nanoscale

Registered charity number: 207890

Nanoscale

PAPER

Cite this: *Nanoscale*, 2016, **8**, 10615

Two-step fabrication of self-catalyzed Ga-based semiconductor nanowires on Si by molecular-beam epitaxy†

Xuezhe Yu, Lixia Li, Hailong Wang, Jiaxing Xiao, Chao Shen, Dong Pan and Jianhua Zhao*

Received 7th November 2015,
Accepted 18th January 2016

DOI: 10.1039/c5nr07830j

www.rsc.org/nanoscale

For the epitaxial growth of Ga-based III–V semiconductor nanowires (NWs) on Si, Ga droplets could provide a clean and compatible solution in contrast to the common Au catalyst. However, the use of Ga droplets is rather limited except for that in Ga-catalyzed GaAs NW studies in a relatively narrow growth temperature (T_s) window around 620 °C on Si. In this paper, we have investigated the two-step growth of Ga-catalyzed III–V NWs on Si (111) substrates by molecular-beam epitaxy. First, by optimizing the surface oxide, vertically aligned GaAs NWs with a high yield are obtained at T_s = 620 °C. Then a two-temperature procedure is adopted to preserve Ga droplets at lower T_s, which leads to an extension of T_s down to 500 °C for GaAs NWs. Based on this procedure, systematic morphological and structural studies for Ga-catalyzed GaAs NWs in the largest T_s range could be presented. Then within the same growth scheme, for the first time, we demonstrate Ga-catalyzed GaAs/GaSb heterostructure NWs. These GaSb NWs are axially grown on the GaAs NW sections and are pure zinc-blende single crystals. Compositional measurements confirm that the catalyst particles indeed mainly consist of Ga and GaSb sections are of high purity but with a minor composition of As. In the end, we present GaAsSb NW growth with a tunable Sb composition. Our results provide useful information for the controllable synthesis of multi-compositional Ga-catalyzed III–V semiconductor NWs on Si for heterogeneous integration.

1. Introduction

III–V semiconductors have preferable properties such as direct band-gaps for optoelectronics and high carrier mobility for microelectronics in comparison with Si, which is the mainstream of the semiconductor technology. Thus monolithic integration of Si with III–V semiconductors would be an attractive approach for versatile and high-performance devices. However, large lattice mismatches between Si and III–V semiconductors have prevented the latter from high-quality epitaxial growth on Si substrates. On the nanoscale, such a problem can be circumvented owing to the efficient strain relaxation through the nanostructure surface, *e.g.* nanowires.[1]

III–V semiconductor nanowires (NWs) have been the focus of substantial research interest due to their promising potentials as new building blocks of nanoelectronics and optoelectronics.[2–6] The one-dimensional growth is usually triggered by a vapor–liquid–solid (VLS) mechanism with the Au catalyst.[7] However, there are only a few reports of Au-catalyzed III–V NWs grown on Si,[8–11] possibly due to the difficulty in controlling the surface properties of Si and the chemical stability of the Au particle. For the robust growth of III–V NWs on Si, several methods have been proposed such as buffer layer deposition before III–V NW growth on Si,[12,13] selective-area growth[14] and using a metal catalyst other than Au, *e.g.* Ag as demonstrated by our earlier work.[15] Among them, the Ga-catalyzed method is particularly suitable for the epitaxial growth of III–V NWs on Si due to the clean growth process (*e.g.* avoiding the common Au impurities in NWs[16,17]) and the easy maneuverability on Si, which brings the highly interesting possibility of the seamless integration of III–V semiconductors with Si.[2] In this perspective, Ga droplets are expected to act as an appropriate catalyst for VLS fabrication of Ga-based binary and ternary III–V NWs for rational band-gap engineering. However, among the various Ga-V NWs, only GaAs NWs have been studied in a limited growth temperature (T_s) range around 620 °C on Si[18–28] and the use of Ga droplets is still lacking. Several attempts have been made but they could not reach pure Ga-V NWs and thus revealed a limited ability to adjust the composition.[29–31]

State Key Laboratory of Superlattices and Microstructures, Institute of Semiconductors, Chinese Academy of Sciences, P.O. Box 912, Beijing 100083, China. E-mail: jhzhao@red.semi.ac.cn

†Electronic supplementary information (ESI) available. See DOI: 10.1039/c5nr07830j

In this paper, the molecular-beam epitaxy (MBE) growth of Ga-catalyzed III–V NWs at low temperatures on Si (111) substrates has been systematically investigated. First, we have optimized the surface oxide on Si substrates to achieve a high yield of vertical GaAs NWs at the normal growth temperature of 620 °C. By a two-temperature procedure, Ga droplets could persist even at 500 °C, and we have realized GaAs NW growth at that low temperature. The morphology and crystal structure of Ga-catalyzed GaAs NWs grown in the largest T_s window so far have been studied. Then using the same growth procedure, we have successfully fabricated Ga-catalyzed GaAs/GaSb heterostructural NWs. These GaSb sections are perfect zinc-blende with a small amount of As composition due to our usage of an As_4 source in the growth. It is also confirmed that the seed particles mainly consist of Ga acting as a catalyst. The growth of Ga-catalyzed GaAsSb NWs is also presented to show that Sb could be tunable. Our results present that the Ga droplets are reliable for the controlled growth of III–V compound semiconductor NWs on Si for heterogeneous integration.

2. Experimental details

NW growth was carried out on Si(111) substrates by MBE. We used a special treatment for substrates. Specifically, at first, we removed the native SiO_2 layer completely using a HF solution of 5%. Then the substrate was coated with a new oxidized layer by dipping the Si substrate in a solution of H_2SO_4 (98%) and H_2O_2 (30%) (volume ratio = 4 : 1).

For the growth of GaAs NWs, both the one-temperature and two-temperature procedures were implemented. The specific growth parameters are listed in Table 1. We used an As_4 source with a fixed beam flux of 6.0×10^{-6} mbar.

We grew GaSb NWs at 490 °C for 40 min after the growth of GaAs NWs at 620 °C for 10 min. The Sb/Ga beam equivalent pressure (BEP) ratio is 2 and that of As/Ga is 6. We used an As_4 flux of 3.0×10^{-6} mbar for this growth and the background pressure due to As_4 is 1×10^{-7} mbar during GaSb growth. In practice, we opened Ga and As (Sb) shutters simultaneously for GaAs (GaSb) NW growth.

The morphology and crystal structure of GaAs and GaSb NWs were characterized by scanning electron microscopy (SEM, Hitachi S-4800) and transmission electron microscopy (TEM, G20 operated at 200 kV and F30 operated at 300 kV). The X-ray energy-dispersive spectroscopy (EDX) measurements were carried out by using F30 equipment.

Table 1 Summary of growth parameters for GaAs NWs. GD is the short for growth duration and BEP stands for beam equivalent pressure

	V/III BEP ratio	First T_s (°C)	First GD (min)	Second T_s (°C)	Second GD (min)
GaAs one-temperature	12	620–520	40	—	—
GaAs two-temperature-A	4	620	10	560–500	30
GaAs two-temperature-B	12	620	10	560–500	30

3. Results and discussion

3.1. Influence of the surface oxide on Ga droplet formation

At first, we demonstrate the achievement of a high yield of Ga-catalyzed GaAs NWs by adopting our substrate preparation method, *i.e.* the re-oxidation method which takes advantage of the fact that Si can be easily oxidized. We compared it with the direct etching method[19,24] and presented the influence on the growth of GaAs NWs in Fig. 1. It is shown that direct etching easily leads to NWs with a significant diversity in length and surface density due to the non-uniform oxide layer caused by an unstable etching rate (Fig. 1(a and b)). The advantage of re-oxidation over direct etching is the generation of a uniformly coated wafer-scale oxide layer on the Si substrate. Using the same NW growth conditions, GaAs NWs on the re-oxidized Si substrate show an optimized morphology with a highly uniform surface density (Fig. 1(c and d)). It has been shown that a change in the native oxide thickness is accompanied by a variation of the surface energy, which determines the contact angle of Ga droplets on the surface and the capability of forming NWs as well as their orientation.[32–34] In this study, we controlled the thickness by adjusting the dipping duration of the Si substrate (ESI, Fig. S1†), which could generate Ga droplets uniformly with a contact angle of 99° (inset of Fig. 1(d)). It is close to the optimal value in ref. 32, indicating an improved efficiency for the formation of Ga droplets on the substrate.

3.2. GaAs NW growth at low temperatures

In order to rule out the discrepancy caused by different MBE systems, the T_s dependence of GaAs NWs was investigated at first and one-temperature samples were grown in our MBE system. As shown in Fig. 2(a–d), NWs only occur sparsely and exhibit a large variance in the length and direction as the T_s goes lower than 600 °C, which is in contrast to the reported T_s window ranging from 400 to 600 °C for Au-catalyzed GaAs NWs.[35] These above results indicate the failed GaAs NW growth on the Si substrate at a T_s lower than 600 °C.

To obtain GaAs NWs in a wide T_s range, we conducted a two-temperature procedure, *i.e.* an appropriate T_s is first adopted to form the base of the NWs and the subsequent growth procedure is done at another T_s.[36] In this case, we found that the preservation of Ga droplets significantly depends on the V/III BEP ratio used. The morphologies of the two-temperature-A series (V/III BEP ratio = 4, see the Experimental details for growth) are presented in Fig. 3(a–c). Compared with the one-temperature series, we clearly see the axial growth at all T_s including even 500 °C, showing the well-behaved catalytic function and the preservation of the Ga droplet at low T_s. These NWs are all vertically aligned and uniformly distributed (Fig. 3(d)). However, for another implementation, *i.e.* the two-temperature-B series (V/III BEP ratio = 12), such an axial growth at low T_s does not happen and only the base NWs remain as shown in Fig. 3(e and f), which is caused by Ga droplet crystallization (Fig. 3(g) and the inset).

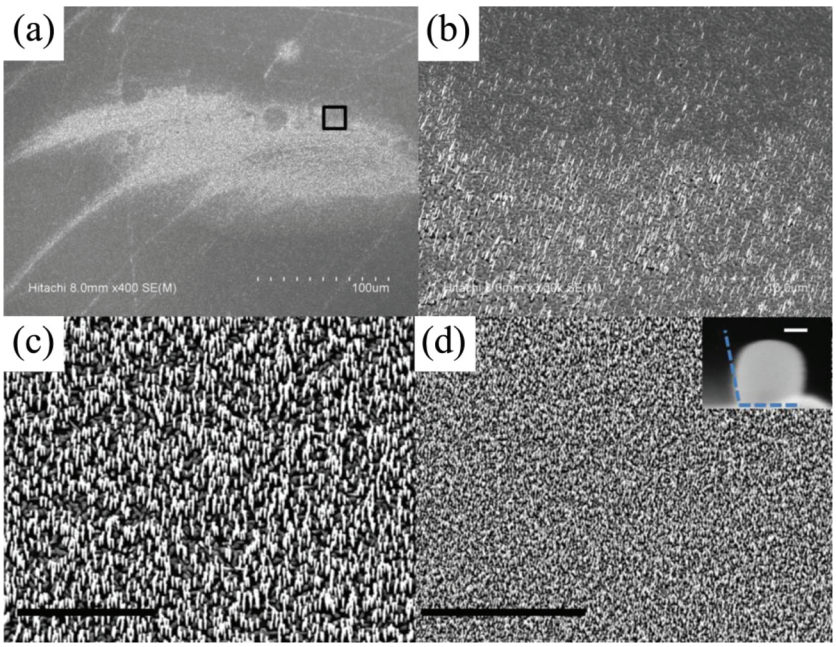

Fig. 1 (a) SEM images of GaAs NWs with the Si substrate covered by a non-uniform oxide layer. (b) Magnified image of the black square in (a). (c and d) Two differently scaled SEM images of GaAs NWs from the same sample with the substrate treated by the re-oxidation method. The scale bars represent 10 μm for (c) and 30 μm for (d), respectively. The inset in (d) is a picture of a Ga droplet before NW growth on the re-oxidized Si and the scale bar is 20 nm.

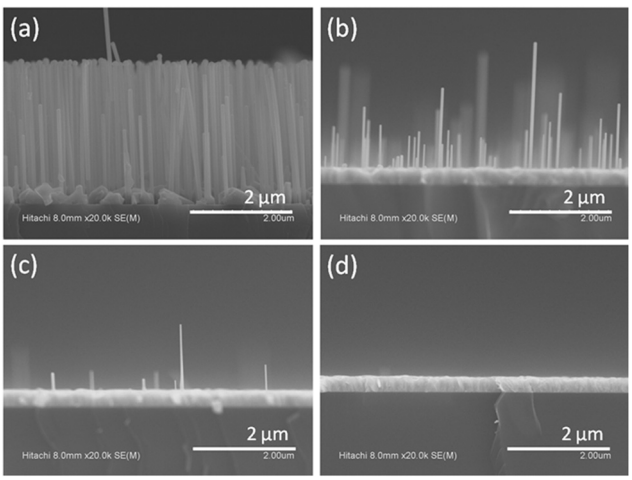

Fig. 2 SEM images of GaAs NWs grown by a one-temperature procedure at (a) 620 °C, (b) 560 °C, (c) 540 °C and (d) 520 °C for 40 min.

From GaAs NWs grown at low T_s, we could further extract the characteristics of Ga-catalyzed NWs. We summarize the growth rates of GaAs NWs grown at all T_s in Fig. 4(a) and divide them into three regions. In region I, the surface diffusion of Ga adatoms limits NW growth, where the growth rate depends on the T_s of the Au-catalyzed GaAs NWs.[37] It can also be seen from Fig. 4(b), which shows the tapering of GaAs NWs grown at low T_s due to the limited diffusion of Ga atoms on the surface of substrates and the sidewall of NWs. As for GaAs NWs grown at high T_s, the radial growth on NW sidewalls is rather uniform. In region II, the growth rate is almost independent of the T_s. In fact, enhanced Ga diffusion increases the amount of the Ga supplement and the As flux begins to limit GaAs NW growth.[20,28] It is also where nearly all the investigations of Ga-catalyzed GaAs NWs are focused on. In region III, GaAs decomposition begins to limit the NW growth due to high T_s (see the ESI†).

Another characteristic of GaAs NWs using Ga droplets at low T_s is manifested in the crystal structure. TEM measurements were carried out for two-temperature-A series. For Au-catalyzed GaAs NWs, the two-temperature procedure remarkably reduces the twin-plane defects.[36] However, an opposite tendency is observed in our samples. For those grown at 620 °C, the crystal structure is a high quality zinc-blende (Fig. 5(a)), consistent with the results of others.[20,21,25,26] Nevertheless, as the T_s is lowered down to 500 °C, the density of twin-plane defects significantly increases (Fig. 5(b–e)), and for those grown at 500 °C, even the wurtzite phase appears in the NW body (Fig. 5(f)). The streaks in the selected area diffraction (SAD) (the inset of Fig. 5(e)) also show the high density of twin-plane defects and a low crystal quality compared with that grown at 620 °C (the inset of Fig. 5(a)). Based on the analysis of the surface diffusion limited growth mentioned above, the observation is probably due to the triple phase line shift caused by a decrease of the Ga droplet volume,[20] which is induced by the suppressed diffusion of Ga adatoms at low T_s. This can be further verified by growing GaAs NWs with an inverse two-temperature procedure, where the crystal structure is still a high-quality zinc-blende (see the ESI†).

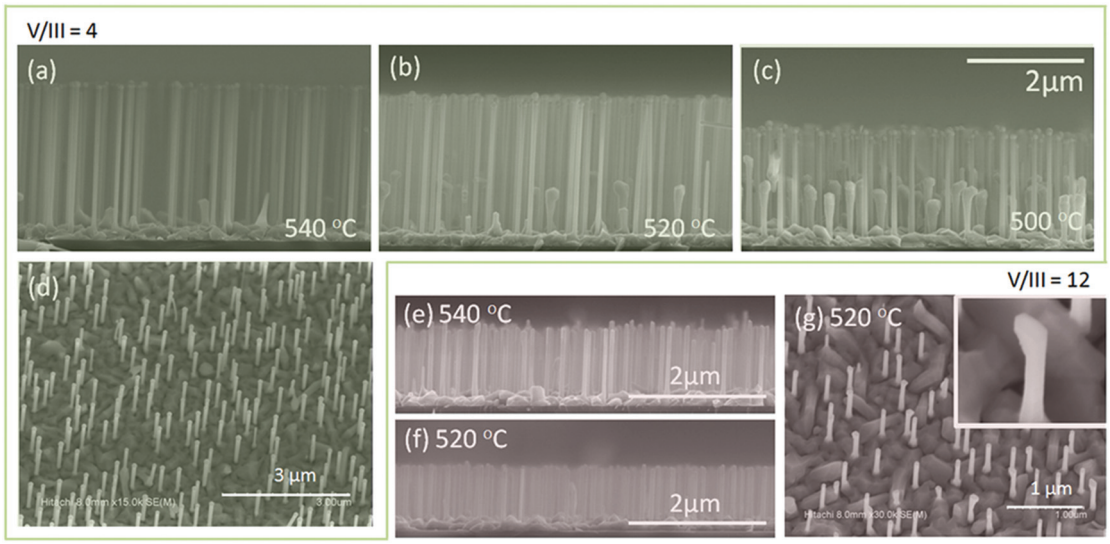

Fig. 3 SEM images of GaAs NWs for a two-temperature series with a V/III BEP ratio of 4 (a–d) and 12 (e–g). The scale bars of (a and b) are the same as that of (c). (d) and (g) Typical top view images for the two series. The inset in (g) shows the crystallization of Ga droplets.

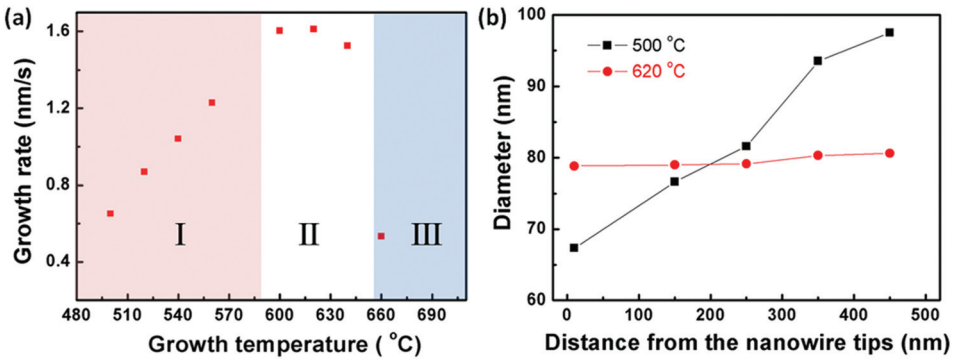

Fig. 4 (a) The growth rate *versus* growth temperature plot for Ga-catalyzed GaAs NWs. (b) Plot of GaAs NW diameters at different positions in the NWs grown at 620 °C and 500 °C.

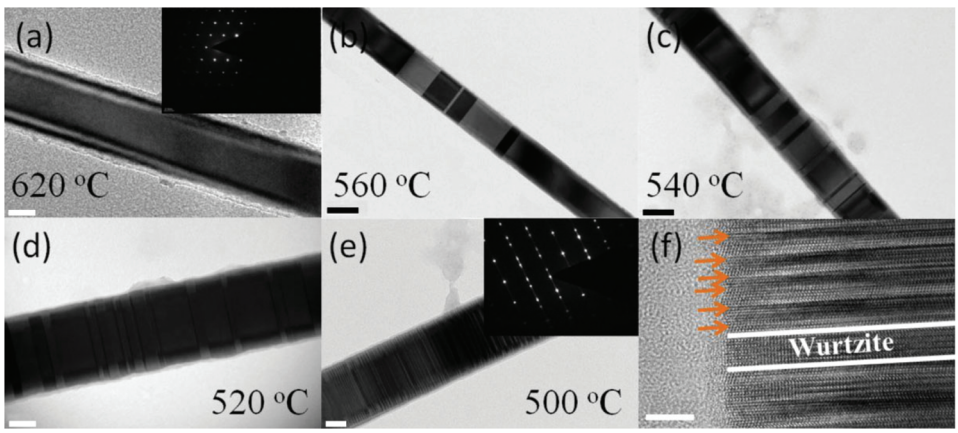

Fig. 5 TEM images for two-temperature-A series samples grown at (a) 620 °C, (b) 560 °C, (c) 540 °C, (d) 520 °C and (e) 500 °C respectively. (f) High-resolution TEM image of a NW grown at 500 °C. The twin-plane defects (by orange arrows) and a section of the wurtzite phase are indicated. The insets of the (a) and (e) are the corresponding SAD images. The scale bars are 20 nm for (a, d and e), 50 nm for (b and c) and 5 nm for (f).

3.3. GaSb NW growth

Although Au-catalyzed GaSb NWs and Ga-catalyzed $GaAs_{1-x}Sb_x$ NWs were reported before,[30,38,39] the MBE growth of Ga-catalyzed GaSb NWs has not been realized yet. Here, making use of the Ga droplets, GaSb NWs were synthesized. The morphology of a typical Ga-catalyzed GaAs/GaSb heterostructural NW is presented in Fig. 6(a). The GaSb section has a wider diameter compared to that of the GaAs section. We also observe that the GaSb section is a pure zinc-blende, which is shown by high resolution TEM and SAD (Fig. 6(b) and inset). EDX along the axial direction shows that the catalyst is mainly composed of Ga and almost no Sb or As is found, confirming that GaSb section growth is triggered by Ga droplets (Fig. 6(c) and (d)). EDX scanning along the cross-axial direction shows that As is present in a small amount of around 4% in the GaSb NW body, which is probably caused by the background pressure due to our usage of an As_4 source (Fig. 6(e)). More EDX data can be found in the ESI.† Since we have fabricated GaAs NWs and GaSb NWs at similar growth temperatures, intuitively we expect no fundamental difficulties in GaAsSb NW growth for band engineering. As GaAsSb NWs with low Sb content have been reported,[30,39] we focus on those with high Sb content. An As background was intentionally utilized for this purpose. We increased it to 3.9×10^{-7} and 5.7×10^{-7} with other growth parameters the same as those for GaSb NWs. The results are presented in Fig. 7 (II and III respectively). Compared with the GaSb NWs (I), we observe that a larger As background leads to longer NWs. EDX measurements show that the Sb composition is 73% (58%) for sample II (III). A more detailed study of GaAsSb NWs will be presented elsewhere. Although GaSb NW and GaAsSb NW growth needs to be further optimized, our

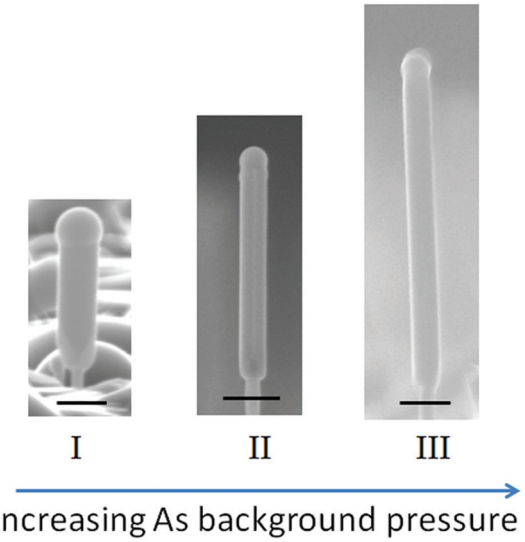

Fig. 7 GaAsSb NWs with different Sb compositions obtained by increasing the As background pressure. Sb percentages of II and III are 73% and 58%, respectively. All three scale bars represent 300 nm. For comparison GaSb NWs (I) with minor As are also presented together.

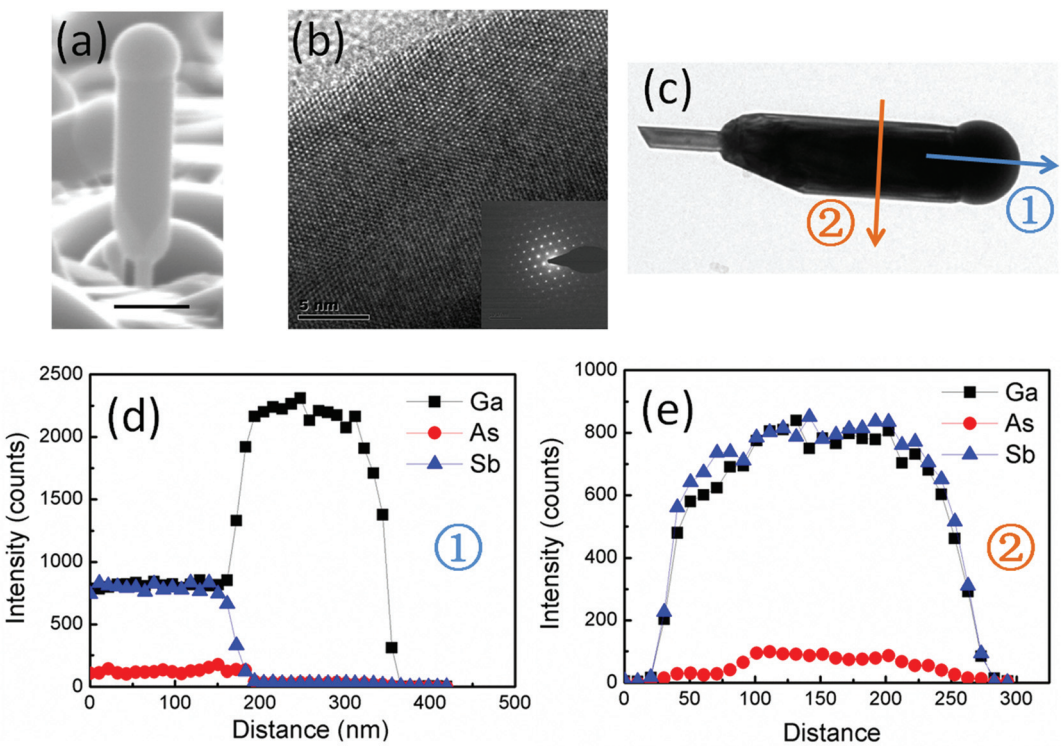

Fig. 6 (a) A typical SEM image of the GaSb section, of which the scale bar represents 300 nm. (b) High resolution TEM of a GaSb NW. The inset is the SAD image from the same GaSb NW. (c) TEM image of a GaSb section showing the directions of EDX line scans. (d) and (e) are the corresponding EDX line scans along the axial and cross-axial directions, respectively.

results clearly show the potential of Ga droplets as an appropriate catalyst for the growth of Ga-based binary and ternary III–V semiconductor NWs on Si substrates.

4. Conclusion

In conclusion, we have investigated the two-temperature growth of Ga-catalyzed GaAs and GaSb NWs on Si(111) by MBE. We first optimize the surface oxide on Si to produce a high yield of vertical GaAs NWs at 620 °C. Then we adopt a two-temperature procedure to preserve Ga droplets for further Ga-catalyzed NW growth. The morphology and crystal structure of GaAs NWs grown at a low temperature are investigated thoroughly. Subsequently the same approach has been transferred readily to the growth of GaSb NWs, which is a pure zinc-blende. EDX measurements show that the catalyst is the Ga droplet and the fabricated GaSb NWs are of high purity. Tuning of the Sb composition in GaAsSb is also presented. The ability to synthesize III–V NWs using Ga droplets on Si substrates provides useful information for the seamless integration of Si technology with the functional III–V semiconductor materials.

Acknowledgements

X. Z. Yu would like to acknowledge the support from Youth Innovation Promotion Association, CAS and also from NSFC (Grant No. 61404127). J. H. Zhao thanks MOST of China for Grant 2012CB932701.

References

1 T. Martensson, C. P. T. Svensson, B. A. Wacaser, M. W. Larsson, W. Seifert, K. Deppert, A. Gustafsson, L. R. Wallenberg and L. Samuelson, *Nano Lett.*, 2004, **4**, 1987.
2 K. A. Dick and P. Caroff, *Nanoscale*, 2014, **6**, 3006.
3 K. Tomioka, M. Yoshimura and T. Fukui, *Nature*, 2012, **488**, 189.
4 J. Wallentin, N. Anttu, D. Asoli, M. Huffman, I. Aberg, M. H. Magnusson, G. Siefer, P. Fuss-Kailuweit, F. Dimroth, B. Witzigmann, H. Q. Xu, L. Samuelson, K. Deppert and M. T. Borgstrom, *Science*, 2013, **339**, 1057.
5 P. Krogstrup, H. I. Jørgensen, M. Heiss, O. Demichel, J. V. Holm, M. Aagesen, J. Nygard and A. Fontcuberta I Morral, *Nat. Photonics*, 2013, **7**, 306.
6 H. J. Joyce, Q. Gao, H. H. Tan, C. Jagadish, Y. Kim, M. A. Fickenscher, S. Perera, T. B. Hoang, L. M. Smith, H. E. Jackson, J. M. Yarrison-Rice, X. Zhang and J. Zou, *Adv. Funct. Mater.*, 2008, **18**, 3794.
7 R. S. Wagner and W. C. Ellis, *Appl. Phys. Lett.*, 1964, **4**, 89.
8 X. Y. Bao, C. Soci, D. Susac, J. Bratvold, D. P. R. Aplin, W. Wei, C. Y. Chen, S. A. Dayeh, K. L. Kavanagh and D. L. Wang, *Nano Lett.*, 2008, **8**, 3755.
9 K. A. Dick, K. Deppert, L. Samuelson, L. R. Wallenberg and F. M. Ross, *Nano Lett.*, 2008, **8**, 4087.
10 A. L. Roest, M. A. Verheijen, O. Wunnicke, S. Serafin, H. Wondergem and E. P. A. M. Bakkers, *Nanotechnology*, 2006, **17**, S271.
11 S. G. Ihn, J. I. Song, T. W. Kim, D. S. Leem, T. Lee, S. G. Lee, E. K. Koh and K. Song, *Nano Lett.*, 2007, **7**, 39.
12 H. Huang, X. M. Ren, X. Ye, J. W. Guo, Q. Wang, Y. S. Yang, S. W. Cai and Y. Q. Huang, *Nano Lett.*, 2010, **10**, 64.
13 J. H. Kang, Q. Gao, H. J. Joyce, H. H. Tan, C. Jagadish, Y. Kim, D. Y. Choi, Y. Guo, H. Xu, J. Zou, M. A. Fickenscher, L. M. Smith, H. E. Jackson and J. M. Yarrison-Rice, *Nanotechnology*, 2010, **21**, 035604.
14 K. Tomioka, Y. Kobayashi, J. Motohisa, S. Hara and T. Fukui, *Nanotechnology*, 2009, **20**, 145302.
15 D. Pan, M. Fu, X. Yu, X. Wang, L. Zhu, S. Nie, S. Wang, Q. Chen, P. Xiong, S. von Molnár and J. H. Zhao, *Nano Lett.*, 2014, **14**, 1214.
16 J. E. Allen, E. R. Hemesath, D. E. Perea, J. L. Lensch-Falk, Z. Y. Li, F. Yin, M. H. Gass, P. Wang, A. L. Bleloch, R. E. Palmer and L. J. Lauhon, *Nat. Nanotechnol.*, 2008, **3**, 168.
17 M. Bar-Sadan, J. Barthel, H. Shtrikman and L. Houben, *Nano Lett.*, 2012, **12**, 2352.
18 J. Paek, T. Nishiwaki, M. Yamaguchi and N. Sawaki, *Phys. Status Solidi C*, 2009, **6**, 1436.
19 A. Fontcuberta I Morral, C. Colombo, G. Abstreiter, J. Arbiol and J. R. Morante, *Appl. Phys. Lett.*, 2008, **92**, 063112.
20 X. Z. Yu, H. L. Wang, J. Lu, J. H. Zhao, J. Misuraca, P. Xiong and S. von Molnár, *Nano Lett.*, 2012, **12**, 5436.
21 P. Krogstrup, R. Popovitz-Biro, E. Johnson, M. H. Madsen, J. Nygard and H. Shtrikman, *Nano Lett.*, 2010, **10**, 4475.
22 F. Jabeen, V. Grillo, S. Rubini and F. Martelli, *Nanotechnology*, 2008, **19**, 275711.
23 X. Z. Yu, H. L. Wang, D. Pan, J. H. Zhao, J. Misuraca, S. von Molnár and P. Xiong, *Nano Lett.*, 2013, **13**, 1572.
24 C. Colombo, D. Spirkoska, M. Frimmer, G. Abstreiter and A. Fontcuberta I Morral, *Phys. Rev. B: Condens. Matter*, 2008, **77**, 155326.
25 G. Cirlin, V. Dubrovskii, Y. B. Samsonenko, A. Bouravleuv, K. Durose, Y. Y. Proskuryakov, B. Mendes, L. Bowen, M. Kaliteevski and R. Abram, *Phys. Rev. B: Condens. Matter*, 2010, **82**, 035302.
26 V. G. Dubrovskii, G. E. Cirlin, N. V. Sibirev, F. Jabeen, J. C. Harmand and P. Werner, *Nano Lett.*, 2011, **11**, 1247.
27 S. Plissard, K. A. Dick, G. Larrieu, S. Godey, A. Addad, X. Wallart and P. Caroff, *Nanotechnology*, 2010, **21**, 385602.
28 M. R. Ramdani, J. C. Harmand, F. Glas, G. Patriarche and L. Travers, *Cryst. Growth Des.*, 2012, **13**, 91.
29 Y. Y. Zhang, M. Aagesen, J. V. Holm, H. I. Jorgensen, J. Wu and H. Y. Liu, *Nano Lett.*, 2013, **13**, 3897.
30 S. Plissard, K. Dick, X. Wallart and P. Caroff, *Appl. Phys. Lett.*, 2010, **96**, 121901.
31 Y. Araki, M. Yamaguchi and F. Ishikawa, *Nanotechnology*, 2013, **24**, 065601.

32 F. Matteini, G. Tütüncüoglu, H. Potts, F. Jabeen and A. Fontcuberta I Morral, *Cryst. Growth Des.*, 2015, **15**, 3105.
33 E. Russo-Averchi, J. Vukajlovic Plestina, G. Tütüncüoglu, F. Matteini, A. Dalmau-Mallorqui, M. de la Mata, D. Rüffer, H. A. Potts, J. Arbiol, S. Conesa-Boj and A. Fontcuberta I Morral, *Nano Lett.*, 2015, **15**, 2869.
34 F. Matteini, G. Tütüncüoglu, D. Rüffer, E. Alarcón-Lladó and A. Fontcuberta I Morral, *J. Cryst. Growth*, 2014, **404**, 246.
35 M. C. Plante and R. R. LaPierre, *Nanotechnology*, 2008, **19**, 495603.
36 H. J. Joyce, Q. Gao, H. H. Tan, C. Jagadish, Y. Kim, X. Zhang, Y. Guo and J. Zou, *Nano Lett.*, 2007, **7**, 921.
37 V. G. Dubrovskii, N. V. Sibirev, R. A. Suris, G. E. Cirlin, J. C. Harmand and V. M. Ustinov, *Surf. Sci.*, 2007, **601**, 4395.
38 Y. N. Guo, J. Zou, M. Paladugu, H. Wang, Q. Gao, H. H. Tan and C. Jagadish, *Appl. Phys. Lett.*, 2006, **89**, 231917.
39 S. Conesa-Boj, D. Kriegner, X. L. Han, S. Plissard, X. Wallart, J. Stangl, A. Fontcuberta I Morral and P. Caroff, *Nano Lett.*, 2014, **14**, 326.